A New Member of the Thioredoxin Reductase Family from Early Oxygenic Photosynthetic Organisms

Rubén M. Buey[1], Sergio Galindo-Trigo[2†], Luis López-Maury[3], Adrián Velázquez-Campoy[4], José Luis Revuelta[1], F. Javier Florencio[3], José M. de Pereda[5], Peter Schürmann[6], Bob B. Buchanan[7], Monica Balsera[2,8]

[1]Dept. Microbiología y Genética. Universidad de Salamanca, Salamanca, Spain; [2]Instituto de Recursos Naturales y Agrobiología de Salamanca (IRNASA-CSIC), Salamanca, Spain; [3]Instituto de Bioquímica Vegetal y Fotosíntesis (CSIC-Universidad de Sevilla), Sevilla, Spain; [4]Institute of Biocomputation and Physics of Complex Systems (BIFI), University of Zaragoza, Zaragoza, Spain; [5]Instituto de Biología Molecular y Celular del Cáncer (CSIC-Universidad de Salamanca), Salamanca, Spain; [6]Laboratoire de Biologie Moléculaire et Cellulaire, Université de Neuchâtel, Neuchâtel, Switzerland; [7]Department of Plant & Microbial Biology, University of California, Berkeley, USA; [8]Corresponding author: monica.balsera@csic.es

Dear Editor,

Thioredoxins (Trxs) are key components of the redox system that regulates the activity of a spectrum of target proteins through dithiol-disulfide exchange reactions. Trxs are reduced by members of the Trx reductase (TR) family (Jacquot et al., 2009). NADP-dependent Thioredoxin Reductases (NTRs), the most common type, belong to the family of dimeric pyridine nucleotide disulfide oxidoreductase flavoproteins that use NADPH as the source of reducing equivalents. In oxyphotosynthetic organisms, in particular, NTRs coexist with the ferredoxin/thioredoxin system (FTS), composed of ferredoxin (Fdx), ferredoxin:thioredoxin reductase (FTR) and a Trx. FTRs convert the electron signal obtained from photoreduced Fdx to a thiol signal via a 4Fe-4S center and a redox-active disulfide catalytic center. FTR, in turn, reduces Trx.

In cyanobacteria and chloroplasts, the FTS is closely associated with the regulation of enzymes of the Calvin-Benson cycle and associated processes—e.g., the oxidative pentose

[*] Dedicated to the memory of David B. Knaff who made major contributions to the biochemistry of flavin enzymes and proteins engaged in redox regulation by thiol transitions.

[†] Current address: Department of Animal and Plant Sciences, University of Sheffield, Sheffield, UK.

phosphate pathway (Balsera et al., 2014). In contrast to other oxygenic photosynthetic organisms, the ancient cyanobacterium *Gloeobacter* and the ocean-dwelling green oxyphotobacteria *Prochlorococcus* lack an FTR gene. This observation raises the question of how these photosynthetic organisms link the Calvin-Benson cycle and related metabolic processes to light and other changing environmental conditions.

To gain information on this point, we have conducted a comparative analysis of NTR-like Trx reductase protein sequences and identified an enzyme common to *Gloeobacter* and green oxyphotobacteria that possibly functions in this connection. The enzyme—provisionally named "DTR" for Deeply-rooted bacterial Thioredoxin Reductase—shows high similarity to NTR but exhibits unique structural features (Figure 1). The enzyme is present in other bacteria, including organisms within the deeply-rooted bacterial lineages as well as marine algae (Table S1; Figure S1). A multiple protein sequence alignment showed that *Gloeobacter* and *Prochlorococcus* DTRs harbor the conserved FAD-binding motif and the two active-site Cys residues typical of authentic NTRs (Figure 1A). Major differences were noted, however, in the amino acids responsible for pyridine nucleotide binding (GxGxxA/G and HRRxxR) (Figure 1A). These included substitutions of crucial residues for coordination to the pyrophosphate group and absence of specific positively charged amino acids needed for electrostatic interactions with the 2´-phosphate group of the adenosine. Additional variations included a C-terminal extension with a conserved aromatic residue, and a fused N-terminal redoxin domain that is restricted to a few bacteria (grey box, Figure S1).

The visible-UV absorption spectrum of purified *Gloeobacter* DTR (GvDTR) showed features typical of a flavoprotein, including absorption maxima at 391 and 459 nm (continuous black line, Figure 1B) (Prongay and Williams, 1992). In contrast to NTRs, the *Gloeobacte*r flavoprotein failed to show activity in the assay of the enzyme in which NAD(P)H oxidation is coupled to the reduction of 5,5´-dithiobis(2-nitrobenzoic acid) (DTNB) (Figure 1C) (Holmgren and Bjornstedt, 1995). The apparent lack of activity could be due to either of two reasons. One, NAD(P)H reduces FAD, but electrons are not further shuttled to the non-physiological substrate DTNB. Alternatively, the flavoprotein does not function with NAD(P)H.

To distinguish between these possibilities, we applied isothermal titration calorimetry (ITC) as a direct approach for assessing protein-ligand binding. For these experiments, we included 3-acetylpyridine adenine dinucleotide phosphate (AADP), a non-hydrolyzable analog of NADPH, that binds tightly to NAD(P)-dependent enzymes. In contrast to *Escherichia coli* NTR (EcNTR) that binds $NADP^+$ and $AADP^+$ with a K_d in the micromolar range, the *Gloeobacter* protein failed to bind either ligand *in vitro* (Figure 1D and Table S2). The lack of affinity for pyridine nucleotides resembles TR from the archeon *Thermoplasma acidophilum* (TaTR; Hernandez et al., 2008), although structural differences were detected between the two proteins. GvDTR displayed a modified GxGxxA/G structural pattern for nucleotide binding (Figure S2, red box), and contained a C-terminal extension missing in TaTR (Figure S2, green box).

To confirm that the *Gloeobacter* flavoprotein fulfills the function of a TR, we determined whether it could reduce Trx dithionite as artifical electron donor. Trx m (also known as TrxA) is the only canonical Trx form in *Gloeobacter* and *Prochlorococcus* (Balsera et al., 2014; Florencio et al., 2006). We observed that dithionite was able to slowly reduce the flavoenzyme anaerobically as measured by a decrease in absorbance at 459 nm (Figure 1B). Partial reoxidation of the enzyme was observed immediately after adding *Gloeobacter* Trx as seen by recovery of the main features of the visible-UV spectrum. These results provide evidence that the *Gloeobacter* flavoprotein has Trx reductase activity and functions independently of pyridine nucleotides.

To gain information on the molecular properties of DTR, we determined a high-resolution structure of the *Gloeobacter* protein by X-ray crystallography at 1.9 Å resolution (PDB code 5J60; Table S3). The crystal structure revealed that GvDTR is a homodimer and that each monomer adopts a typical NTR fold (Figure 1E). Despite the high similarity between the FAD- and *pseudo* NADPH-binding domains with those of authentic NTRs, the relative orientation of the domains in the crystal structure differed from the flavin-oxidizing (FO) and flavin-reducing (FR) conformations found in NTRs (Lennon and Williams, 1997) (Figure S3). No direct interaction was observed between amino acids of the *pseudo* NADPH-binding domains, as detected between the two corresponding domains in the NTR dimer both in FO and FR conformations, suggesting that the two functional domains in DTRs are flexible relative to each other. FAD in GvDTR was found to be oxidized based on the planar conformation and the yellow color of the crystal. The redox-active Cys

residues were reduced and distant from the *re* face of the isoalloxazine ring instrumental for electron transfer (Figure 1E).

Coordination to the FAD cofactor is well conserved compared to NTRs of known 3D structure (Figure S4). However, analysis of the NADPH-binding pocket revealed significant structural deviations from NTRs (Figure S5). One of the most striking variations is related to the substitution of the second strictly conserved Gly in the GxGxxA/G motif in EcNTR by an Asn in GvDTR (Figure 1A, red box). GvDTR structure showed that the substrate binding pocket is blocked by the side chain carboxamide of Asn (N154; Figure S5E), supporting the finding that the enzyme does not bind pyridine nucleotides. Remarkably, the aromatic side chain of a tryptophan (W315) in one monomer stacks over the central portion of the FAD isoalloxazine ring of the second monomer on its *re* face (Figure 1E). This position is generally occupied by either the pyridine nucleotide or the disulfide bridge in NTRs. The tryptophan position is highly conserved in the protein sequences of the DTR family, including early branching bacteria, cyanobacteria and marine algae, replaced by a tyrosine residue only in firmicutes and chlorobi (Figure S1), and suggests a potential physiological role for this residue. As displayed here, the C-terminal tail has not previously been reported and is a unique feature of DTR. Relative to WT, deletion of the C-terminal motif in *Gloeobacter* DTR (GvDTR_Δt) was accompanied by ca. a 7-9 nm shift in the flavin absorption maxima in the blue region of the spectrum (Figure 1B, lower panel). More interestingly, removal of the C-terminal tail increased the rate of flavin reduction by dithionite (~ 10-fold) to levels comparable to those with the *E. coli* enzyme (legend Figure 1B). Collectively, these results suggest that the unique C-terminal module on DTR has a direct influence on enzyme activity and might constitute a mechanism of regulation not previously reported.

The C-terminal extension of DTR resembles the C-terminal subdomain of certain ferredoxin-NADP reductase enzymes (FNRs) in which an aromatic residue protrudes over the *re* side of FAD, thereby requiring its displacement for a productive interaction between the pyridine nucleotide and FAD (Ceccarelli et al., 2004). Among the different types of FNRs, structural similarities were detected between DTR and TR-type FNRs. These FNRs harbor conserved FAD and NADPH-binding motifs but lack the redox active Cys. An aromatic residue in a short alpha-helix at the C-terminus protrudes over the *re* side of FAD (Figure S6). Mutational studies in TR-type FNR enzymes have shown that replacement of

the aromatic residue on the *re* face of the flavin perturbs binding with its redox partner (Seo et al., 2014). Following a molecular mechanism similar to these FNRs, displacement of the C-terminal extension of DTR would allow access of the redox disulfide to the *re*-face of FAD likely in a regulatory manner. As for NTRs, conformational flexibility is expected to play an important role in the mechanism of enzyme action. Thus DTR in solution may exist in equilibrium between the structure observed in the crystal and other configurations in which the donor molecule (and/or the disulfide) is in close contact with the flavin group. In light of the high structural similarity with NTRs and the finding that DTR lacks the archetypal NADPH binding site, the physiological donor is thought to be a cofactor acting similar to pyridine nucleotides. Other types of molecules such as small redox carrier proteins can, however, not be excluded. To this point, a ferredoxin-linked flavoprotein enzyme that reduces Trx has been isolated from clostridia (Hammel et al., 1983). In the end, only the identification of the physiological electron donor will clarify the catalytic mechanism of Trx reduction.

In the present study, we have provided evidence for the diversity of Trx systems in bacteria and for variation in the ability of the reductases to deliver electrons to Trx. Our results support the view that the redox systems consist of structural modules and regulatory elements that different organisms have conveniently combined during evolution to create proteins capable of adapting to specific metabolic and environmental situations. They also provide a structural foundation for future exploration of the mechanism of action and open the door to understanding the evolutionary development of different flavin reductases in relation to particular metabolic demands.

Acknowledgements

We thank Dr. Charles H. Williams for a sample of AADP and for suggestions on the manuscript. We thank Dr. Biswarup Mukhopadhyay for EcNTR and EcTrx expression vectors and for scientific discussions. We are grateful to Drs. Luis Rubio and Emilio Jiménez for help and guidance with the dithionite experiments. B.B.B. acknowledges support from an Alexander von Humboldt Research Award that catalyzed the launching of this project at the Ludwig-Maximilians-Universität in Munich. R.M.B. is supported by a ‘Ramón y Cajal’ contract from the Spanish Ministerio de Economía y Competitividad. L. L-M. is supported by a postdoctoral contract from Universidad de Sevilla. Protein

crystallography experiments were performed at the PXIII (SLS, Switzerland) beamline with the collaboration of SLS staff.

References

Balsera, M., Uberegui, E., Schürmann, P., and Buchanan, B.B. (2014). Evolutionary development of redox regulation in chloroplasts. Antioxid. Redox Signal. **21**:1327-1355.

Ceccarelli, E.A., Arakaki, A.K., Cortez, N., and Carrillo, N. (2004). Functional plasticity and catalytic efficiency in plant and bacterial ferredoxin-NADP(H) reductases. BBA-Proteins Proteomics **1698**:155-165.

Florencio, F., Pérez-Pérez, M., López-Maury, L., Mata-Cabana, A., and Lindahl, M. (2006). The diversity and complexity of the cyanobacterial thioredoxin systems. Photosynth. Res. **89**:157-171.

Hammel, K.E., Cornwell, K.L., and Buchanan, B.B. (1983). Ferredoxin/flavoprotein-linked pathway for the reduction of thioredoxin. Proc. Natl. Acad. Sci. U. S. A. **80**:3681-3685.

Hernandez, H., Jaquez, O., Hamill, M., Elliott, S., and Drennan, C. (2008). Thioredoxin reductase from *Thermoplasma acidophilum:* a new twist on redox regulation. Biochemistry **47**:9728-9737.

Holmgren, A., and Björnstedt, M. (1995). Thioredoxin and thioredoxin reductase. In: Methods Enzymol.: Academic Press. 199-208.

Jacquot, J.-P., Eklund, H., Rouhier, N., and Schürmann, P. (2009). Structural and evolutionary aspects of thioredoxin reductases in photosynthetic organisms. Trends Plant Sci. **14**:336-343.

Lennon, B.W., and Williams, C.H. (1997). Reductive half-reaction of thioredoxin reductase from *Escherichia coli*. Biochemistry **36**:9464-9477.

Prongay, A.J., and Williams, C.H. (1992). Oxidation-reduction properties of *Escherichia coli* thioredoxin reductase altered at each active site cysteine residue. J. Biol. Chem. **267**:25181-25188.

Seo, D., Asano, T., Komori, H., and Sakurai, T. (2014). Role of the C-terminal extension stacked on the re-face of the isoalloxazine ring moiety of the flavin adenine dinucleotide prosthetic group in ferredoxin-NADP+ oxidoreductase from Bacillus subtilis. Plant Physiol. Biochem. **81**:143-148.

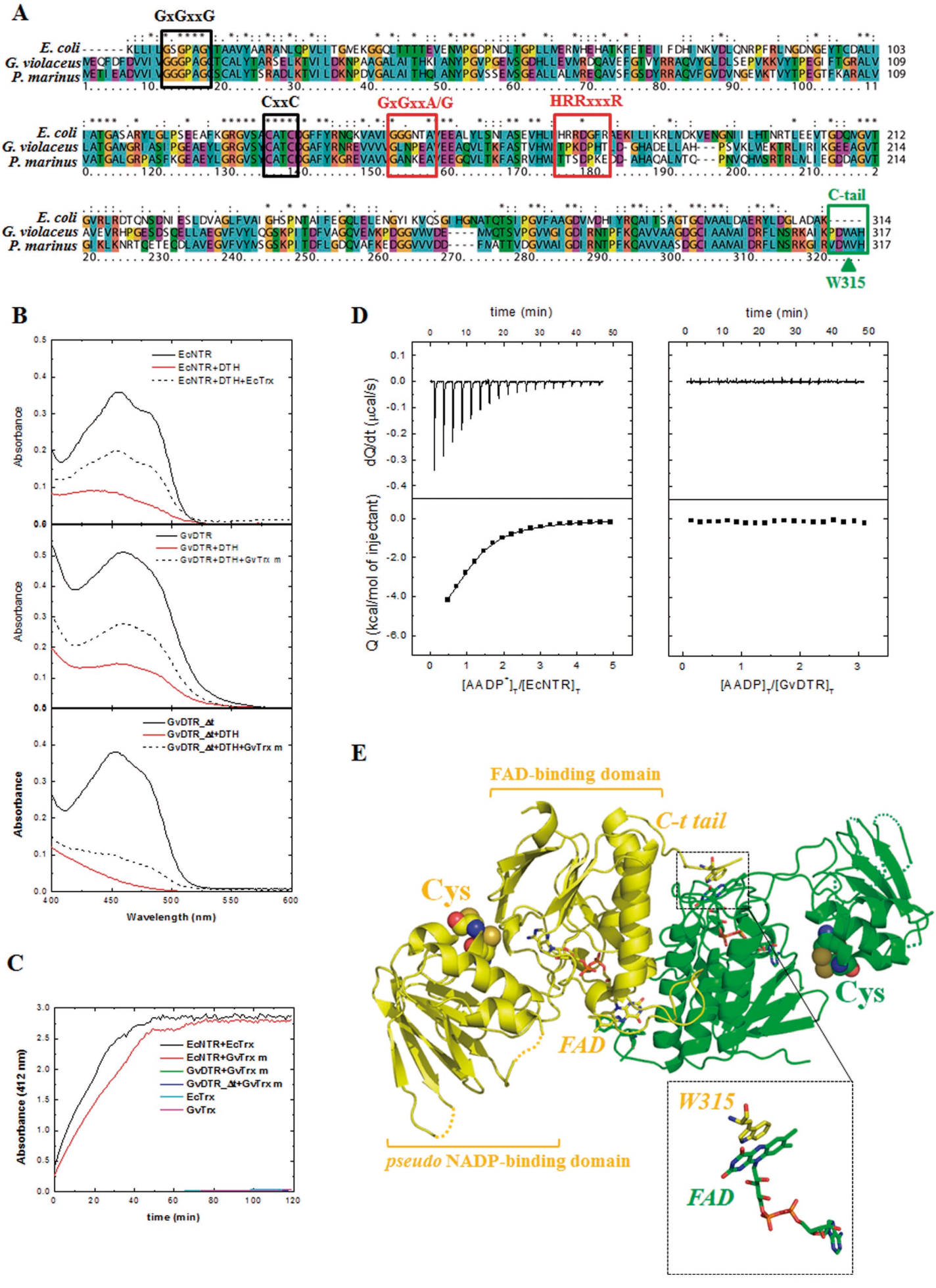
A
GxGxxG
CxxC
GxGxxA/G
HRRxxxR
C-tail
W315
E. coli
G. violaceus
P. marinus
B
EcNTR
EcNTR+DTH
EcNTR+DTH+EcTrx
GvDTR
GvDTR+DTH
GvDTR+DTH+GvTrx m
GvDTR_Δt
GvDTR_Δt+DTH
GvDTR_Δt+DTH+GvTrx m
Absorbance
Wavelength (nm)
C
EcNTR+EcTrx
EcNTR+GvTrx m
GvDTR+GvTrx m
GvDTR_Δt+GvTrx m
EcTrx
GvTrx
Absorbance (412 nm)
time (min)
D
time (min)
dQ/dt (μcal/s)
Q (kcal/mol of injectant)
[AADP•]T/[EcNTR]T
[AADP]T/[GvDTR]T
E
FAD-binding domain
C-t tail
Cys
Cys
FAD
W315
FAD
pseudo NADP-binding domain

Figure 1. (A) Multiple sequence alignment of *Escherichia coli* NTR (EcNTR), *Gloeobacter violaceus* DTR (GvDTR) and *Prochlorococcus marinus* MIT9313 DTR (PmDTR) protein sequences. The motif for FAD binding (GxGxxG) and the redox active Cys (CxxC) are shown with black boxes. Red boxes indicate motifs for NAD(P)H binding (GxGxxA/G and HRRxxxR). At the C-terminal extension (green box), the tryptophan residue is marked with a triangle. Residue conservation colors are shown according to default ClustalX parameters; **(B)** Visible absorption spectra of EcNTR, GvDTR and GvDTR_Δt corresponding to band II, which is associated with the molecular environment and chemical state of the isoalloxazine moiety of the flavin. Flavoenzymes are represented by a black line. Red lines show the flavin absorption spectra after incubation with dithionite (DTH) under anaerobic conditions for the following times: 6 min (EcNTR), 70 min (GvDTR) and 8 min (GvDTR_Δt). The spectra obtained after addition of homologous Trx m to the reduced system (less than 3 min) are displayed as dashed black lines; **(C)** Absorbance changes at 412 nm as a consequence of DTNB reduction using NADPH as source of reducing equivalents for DTR. EcNTR that is active with its homologous Trx (EcTrx) as well as GvTrx m served as control; **(D)** Calorimetric assays for determining the binding affinity of AADP to EcNTR (left panel) and GvDTR (right panel). Thermograms (upper plots) correspond to the heat change in the sample cell associated to the sequential addition of the ligand (AADP) to the protein (EcNTR or GvDTR) ($[ligand]_{Total}/[protein]_{Total}$) relative to a reference cell containing only buffer. At the bottom, the continuous line corresponds to the non-linear regression fitting analysis of the integrated experimental data considering a model function that assumes a single binding site (Table SII); (**E)** Crystal structure of GvDTR homodimers (each monomer represented in yellow and green colors). Missing loops are represented as dashed lines (monomer 2 in green showed poorer electron density in some loop regions than monomer 1). The redox active Cys are reduced in the crystal and are shown in space-fill representation. The aromatic residue (W315) of the C-terminal tail (C-t tail) in one GvDTR monomer stacks over the FAD of the other monomer forming a pi-stacking (depicted as stick model). The inset shows a zoom-view of the tryptophan-FAD interaction.

SUPPLEMENTAL MATERIAL

File S1. Material and Methods.

Protein production and purification. *Gloeobacter* DTR **(**glr0719) and Trx m (sll0623) ORFs were inserted into the pET28a expression vector (Novagen). *Escherichia coli* NTR and Trx, cloned in pTEV5, were a kind gift of Biswarup Mukhopadhyay. Point mutations and deletions were prepared according to (Li et al., 2008). All constructs were corroborated by DNA sequencing. Recombinant proteins were produced in Rosetta (DE3) *E. coli* cell strain, and proteins were purified from the soluble fraction using Ni^{2+} HiPrep (GE Healthcare). The affinity tag was removed with thrombin or tobacco etch virus protease by dialysis. Proteins were further purified by gel filtration chromatography on a HiPrep 16/60 Sephacryl S300 (GE Healthcare) in buffer 50 mM Tris-HCl pH 7.6, 150 mM NaCl and 2 mM β-mercaptoethanol. Flavoproteins were incubated with an excess of FAD (Sigma) before gel filtration, unless otherwise indicated. Protein concentration was measured by the Bradford method (Bradford, 1976).

Enzyme assays. NAD(P)H-dependent TR activity was determined following the reduction of 5,5'-dithiobis(2-nitrobenzoic acid) (DTNB) by measuring the increase in absorbance at 412 nm. The assay mixture contained 0.15 mM NAD(P)H, 5 mM DTNB, 50 nM TR and 5 μM Trx in 100 mM potassium phosphate, 2 mM EDTA, pH 7.0 (Holmgren and Bjornstedt, 1995). Dithionite reduction experiments were performed under anaerobic conditions in buffer 100 mM potassium phosphate pH 6.8, 100 mM KCl and 2 mM EDTA (Prongay and Williams, 1992). Reduction of the flavoprotein (0.05 mM) was monitored in a spectrofluorometer after addition of 0.5 mM sodium dithionite (Sigma). Then, 0.1 mM Trx was added to the reaction mixture and the flavin spectrum was immediately recorded.

Isotermal titration calorimetry (ITC). Standard ITC experiments were performed using an AutoITC200 system (Microcal). Briefly, a 20 μM protein solution in buffer 100 mM potassium phosphate, 2 mM EDTA, pH 7.0 was titrated at 25 °C with a 300-500 μM $NADP^+$, NAD^+ or $AADP^+$ solution. Parallel experiments were performed by injecting the coenzymes into the buffer. The heats of dilution were negligible and subtracted from their respective titrations prior to data analysis. The resulting heats were integrated and fitted with a model for a single ligand binding site implemented in the software package Origin (OriginLab Corporation, Northamptom, MA).

Crystallization and structure determination. Crystals were grown in sitting drops at room temperature using the vapour diffusion method by mixing the protein solution at 10 mg/mL in buffer 10 mM Tris-HCl, 50 mM NaCl and 0.5 mM TCEP with an equal volume of mother liquor consisting in 30 % PEG-400, 0.1 M sodium acetate pH 4.5 and 0.2 M calcium acetate. Protein crystals were flash-cooled in liquid nitrogen and data were collected at 100 K at the PXIII beamline at the Swiss Light Source (PSI, Villigen, Switzerland) using monochromatic X-rays of 1.000 Å wavelength. Diffraction intensities were indexed and integrated by using the software XDS (Kabsch, 2010) and scaled with XSCALE. Diffraction data were phased by molecular replacement using the program Phaser (McCoy et al., 2007) within the CCP4 crystallographic software suite (Potterton et al., 2003) using the crystal structure of NTR from *Deinococcus radiodurans* (PDB code: 2q7v) as template (Obiero et al., 2010). Structure refinement was performed using the PHENIX crystallographic software package (Adams et al., 2010), alternated by visual inspection and manual modelling with Coot (Emsley et al., 2010). Simulated annealing (Cartesian coordinates), gradient-driven positional, restrained individual isotropic B-factor and TLS refinement (Winn et al., 2001) were used for refinement. The refined structures include most of the *Gloeobacter* DTR residues with the exception of short disordered loop regions. 4 FAD, 2 calcium and 2 tetra-ethylene glycol molecules were added to the model. The structure has an excellent geometry with no Ramachandran outliers and 97% of the residues in favored regions (3% in allowed regions). The crystallographic and final refinement statistics are summarized in Table S3. The molecular representations were generated using Pymol (DeLano, 2002). FAD-protein interaction was analyzed by the LigPlot+ program (Laskowski and Swindells, 2011).

Primary structure analysis. DTR homologs were collected from the NCBI database. A protein multiple sequence alignment was performed using ClustalX (Thompson et al., 1997).

Supplemental Bibliography.

Adams, P.D., Afonine, P.V., Bunkoczi, G., Chen, V.B., Davis, I.W., Echols, N., Headd, J.J., Hung, L.W., Kapral, G.J., Grosse-Kunstleve, R.W., et al. (2010). PHENIX: a comprehensive Python-based system for macromolecular structure solution. Acta Crystallogr. D Biol. Crystallogr. **66**:213-221.

Bradford, M.M. (1976). A rapid and sensitive method for the quantitation of microgram quantities of protein utilizing the principle of protein-dye binding. Anal. Biochem. **72**:248-254.

DeLano, W.L. (2002). The PyMOL Molecular Graphics System. Palo Alto, CA: DeLano Scientific.

Emsley, P., Lohkamp, B., Scott, W.G., and Cowtan, K. (2010). Features and development of Coot. Acta Crystallogr. D Biol. Crystallogr. **66**:486-501.

Holmgren, A., and Björnstedt, M. (1995). Thioredoxin and thioredoxin reductase. In: Methods Enzymol.: Academic Press. 199-208.

Kabsch, W. (2010). Xds. Acta Crystallogr D Biol Crystallogr **66**:125-132.

Laskowski, R.A., and Swindells, M.B. (2011). LigPlot+: multiple ligand–protein interaction diagrams for drug discovery. J. Chem. Inf. Model. **51**:2778-2786.

Li, J., Li, C., Xiao, W., Yuan, D., Wan, G., and Ma, L. (2008). Site-directed mutagenesis by combination of homologous recombination and DpnI digestion of the plasmid template in *Escherichia coli*. Anal. Biochem. **373**:389-391.

McCoy, A.J., Grosse-Kunstleve, R.W., Adams, P.D., Winn, M.D., Storoni, L.C., and Read, R.J. (2007). Phaser crystallographic software. J. Appl. Crystallogr. **40**:658-674.

Mulrooney, S.B., and Williams, C.H. (1997). Evidence for two conformational states of thioredoxin reductase from *Escherichia coli*: use of intrinsic and extrinsic quenchers of flavin fluorescence as probes to observe domain rotation. Protein Sci. **6**:2188-2195.

Obiero, J., Pittet, V., Bonderoff, S.A., and Sanders, D.A.R. (2010). Thioredoxin System from *Deinococcus radiodurans*. J. Bacteriol. **192**:494-501.

Potterton, E., Briggs, P., Turkenburg, M., and Dodson, E. (2003). A graphical user interface to the CCP4 program suite. Acta Crystallogr. D Biol. Crystallogr. **59**:1131-1137.

Prongay, A.J., and Williams, C.H. (1992). Oxidation-reduction properties of *Escherichia coli* thioredoxin reductase altered at each active site cysteine residue. J. Biol. Chem. **267**:25181-25188.

Thompson, J.D., Gibson, T.J., Plewniak, F., Jeanmougin, F., and Higgins, D.G. (1997). The CLUSTAL_X windows interface: flexible strategies for multiple sequence alignment aided by quality analysis tools. Nucleic Acids Res. **25**:4876-4882.

Winn, M.D., Isupov, M.N., and Murshudov, G.N. (2001). Use of TLS parameters to model anisotropic displacements in macromolecular refinement. Acta Crystallogr. D Biol. Crystallogr. **57**:122-133.

SUPPLEMENTAL TABLES

Table S1. List of selected species with identified DTR inferred by comparative sequence analysis. The last column shows the species abbreviation name used in this work (see Figure S1).

	Phylum	Species	Abbreviation
BACTERIA	Aquificae	*Aquifex aeolicus*	AQUAE
		Hydrogenobaculum sp. Y04AAS1	HBASP
		Hydrogenivirga sp. 128-5-R1-1	HVISP
		Thermocrinis albus	THEAL
		Thermocrinis ruber	THERU
	Chloroflexi	*Anaerolineae bacterium*	ANABA
		Caldilinea aerophila	CALAE
		Leptolinea tardivitalis	LEPTA
		Thermanaerothirx daxensis	THEDA
	Firmicutes	*Alicyclobacillus pohliae*	ALIPO
		Aeribacillus pallidus	AERPA
		Aneurinibacillus aneurinilyticus	ANEAN
		Aneurinibacillus migulanus	ANEMI
		Bacillus azotoformans	BACAZ
		Bacillus sp. FJAT-27238	BACSP
		Brevibacillus agri	BREAG
		Brevibacillus borstelensis	BREBO
		Brevibacillus brevis	BREBR
		Brevibacillus formosus	BREFO
		Brevibacillus massiliensis	BREMA
		Brevibacillus panacihumi	BREPA
		Brevibacillus sp. BC25	BRESP
		Brevibacillus thermoruber	BRETH
		Caldalkalibacillus thermarum	CALTH
		Effusibacillus pohliae	EFFPO
		Kyrpidia tusciae	KYRTU
		Limnochorda pilosa	LIMPI
		Paenibacillus alginolyticus	PAEAL
		Paenibacillus sp. UNC451MF	PAESP
		Tumebacillus flagellatus	TUMFL
	Chlorobi	*Chlorobium limicola*	CHLLI
		Chlorobium phaeobacteroides	CHLPH
		Prosthecochloris aestuarii	PROAE
	Nitrospirae	*Thermodesulfovibrio islandicus*	THEIS
		Thermodesulfovibrio thiophilus	THETH
		Thermodesulfovibrio yellowstonii	THEYE
	Cyanobacteria	*Acaryochloris marina*	ACAMA
		Acaryochloris sp. CCMEE 5410	ACASP
		Crocosphaera watsonii	CROWA
		Gloeobacter kilaueensis	GLOKI
		Gloeobacter violaceus	GLOVI
		Gloeocapsa sp. PCC 7428	GLOSP
		Leptolyngbya sp. Heron Island J	LEPHE
		Leptolyngbya sp. PCC 7376	LEPPCC
		Pleurocapsa sp. PCC 7327	PLESP
		Prochlorococcus marinus	PROMA

		Rubidibacter lacunae	RUBLA
		Stanieria cyanosphaera PCC 7437	STACY
		Synechococcus sp. PCC 7336	SYNPCC
		Synechococcus sp. CC9902	SYNCC
		Synechococcus sp. WH 8020	SYNWH
		Synechococcus sp. BL107	SYNBL
		Trichodesmium erythraeum	TRIER
EUKARYOTES	Pelagophytes	*Aureococcus anophagefferens*	AURAN
	Diatoms	*Thalassiosira oceanica*	THAOC
	Haptophytes	*Emiliania huxleyi*	EMIHU

Table S2. A summary of dissociation constants (K_d), binding enthalpy (ΔH), and stoichiometry (n) of the flavoenzymes for pyridine nucleotides obtained from ITC experiments. K_d values obtained for *E. coli* NTR were comparable to those reported previously (Mulrooney and Williams, 1997).

	K_d (μM)	ΔH (kcal/mol)	n
EcNTR / $NADP^+$	11	-3.8	1.0
EcNTR / NAD^+	*No interaction*		
EcNTR / $AADP^+$	7.1	-6.8	1.0
GvDTR / $NADP^+$	*No interaction*		
GvDTR / NAD^+	*No interaction*		
GvDTR / $AADP^+$	*No interaction*		

Relative error in *K*d is 15 %; absolute errors in ΔH and n are 0.3 kcal/mol and 0.1, respectively.

Table S3. Data collection and refinement statistics. Statistics for the highest-resolution shell are shown in parentheses.

Wavelength (Å)	1.000
Resolution range (Å)	49.22-1.9 (1.97-1.9)
Space group	P 2_1 2_1 2_1
Unit cell, a, b, c (Å), α, β, γ (°)	83.3 122.0 139.2 90 90 90
Total reflections	1489996 (133884)
Unique reflections	112106 (11092)
Multiplicity	13.3 (12.1)
Completeness (%)	100.00 (100.00)
Mean I/sigma (I)	24.89 (1.97)
Wilson B-factor (Å^2)	32.88
R-merge	0.0654 (1.185)
R-meas	0.0680 (1.237)
R-pim	0.0186 (0.3513)
CC1/2	1 (0.757)
CC*	1 (0.928)
Reflections used in refinement	112069 (11090)
Reflections used for R-free	5593 (531)
R-work	0.1787 (0.2869)
R-free	0.2023 (0.3145)
CC(work)	0.962 (0.850)
CC(free)	0.948 (0.792)
Number of non-hydrogen atoms	9822
macromolecules	8949
ligands	240
solvent	633
Protein residues	1225
RMS bonds(Å)	0.859
RMS angles (°)	6.01

Ramachandran favored (%)	97
Ramachandran allowed (%)	3
Ramachandran outliers (%)	0
Rotamer outliers (%)	0.35
Clashscore	4.07
Average B-factor (Å^2)	47.35
macromolecules (Å^2)	47.93
ligands (Å^2)	31.66
solvent (Å^2)	45.10
Number of TLS groups	23

Supplemental Figures.

Figure S1. Structural features of bacterial DTR protein family (see Table S1 for organism abbreviation). In the amino acid multiple sequence alignment, color and residue conservation are shown according to default ClustalX parameters. The conserved FAD-binding motif (GxGxxG) and the redox active Cys (CxxC) are marked with black boxes. Amino acid regions corresponding to NADP-binding in NTRs (GxGxxA/G and HRRxxxR motifs, are as defined in Figure 1) are depicted in red boxes. The unique C-tail with a conserved aromatic residue in DTR (W or Y, green triangle) is identified in a green box. A few firmicutes contain a redoxin-like domain with a CxxC motif fused at the N-terminus (shown in dashed grey).

Figure S2. Structural comparison of *Gloeobacter violaceus* (GvDTR) with *Thermoplasma acidophilum* TR (TaTR) and *Escherichia coli* NTR (EcNTR). Regions involved in FAD binding (GxGxxG) and the redox active Cys motif (CxxC) are conserved in the three sequences (black boxes). Important differences are noted, however, in the cofactor binding domain. The two NADP-independent TR (GvDTR and TaTR) lack the positive residues for electrostatic interactions with the phosphate group of the adenine ribose present in EcNTR (HRRxxxR motif, marked in red). Different to TaTR and EcNTR, the structural motif GxGxxA/G--strictly conserved in NAD(P)-binding enzymes for coordination to the pyrophosphate group of the pyridine nucleotide (boxed in red)--is not found in GvDTR. Instead, a polar amino acid (asparagine) occupies the position of the second glycine that imposed structural restrictions to cofactor binding as it will be shown in Fig. S6 (D). The C-terminal tail of GvDTR, a peculiar feature of the DTR protein family, is not present in TaTR or in EcNTR.

Figure S3. Structural superposition of the FAD binding domain of GvDTR dimers (each monomer in yellow and green) and EcNTR in the two different catalytic conformations that NTR enzymes experiment during catalysis. **(A)** GvDTR superimposed on FR (flavin reducing) conformation of EcNTR (dimer in blue; PDB code 1trb) in which AADP stacks over FAD for electron transfer; the redox active Cys are exposed to the solvent for interaction with Trx; **(B)** GvDTR superimposed on FO (flavin oxidizing) conformation of EcNTR (dimer in orange, PDB code 1f6m) in which the redox active Cys are positioned over the FAD. Cys are represented in spacefills; AADP and FAD are shown in stick

models. For sake of model completeness, the dimeric model in Figure 1E was built using two monomers of chain A.

Figure S4. Molecular interactions of FAD (in violet) with amino acid residues of GvDTR. Hydrophobic interactions are shown as red arcs. Hydrogen-bond interactions are represented as green dotted lines with bond distances in Å.

Figure S5. Structural differences in the pyridine nucleotide binding region between GvDTR and EcNTR. **(A)** Ribbon diagrams of the structural superposition of GvDTR (magenta; this work) and EcNTR (yellow; PDB code: 1tdf) in the NADP-binding domain. The NADP-binding region (GxGxxG/A and HRRxxxR motifs, Figure S2) is highlighted in green. Disordered loops in GvDTR are represented as dashed lines; **(B)** The side chains of residues corresponding to the glycine-rich region of the NADP-binding motif in GvDTR (GLNPEA, Figure S2) are shown in sticks; **(C)** The glycine-enriched motif for pyridine nucleotide binding of EcNTR (GGGNTA, Figure S2) is shown in sticks; **(D)** NADP bound to EcNTR is shown in sticks (grey backbone trace); **(E)** Surface representation of the NADP binding domain in GvDTR. Asn154 in GvDTR, which substitutes for the second conserved Gly in the GxGxxG/A motif of pyridine nucleotide binding proteins (Figure S2), is represented in sticks; (F) Surface representation of the NADP binding domain in EcNTR. Arg176 and Arg181 in EcNTR involved in electrostatic interactions with the cofactor are shown in sticks and labeled. The binding pocket for NAD(P)H is particularly altered in GvDTR which lacks the residues involved in electrostatic interaction for coordination with the phosphate of NADPH. Most notably, the presence of a polar residue (Asn154) in GvDTR instead of Gly as in true NTRs results in a constricted binding site that would clash with the cofactor, as inferred from a docking model (docked NADP in GvDTR shown in the close-up in E).

Figure S6. Structural similarities between GvDTR and thioredoxin-type FNR. **(A)** GvDTR structure as shown in Fig. S3; **(B)** *Chlorobaculum tepidum* FNR dimer (CtFNR; PDB code: 3ab1). FNR enzymes catalyze NADP reduction via ferredoxin. Different from the plant enzyme, TR-type FNRs show structural similarity to NTRs and contain a C-terminal helix that facilitates the interaction of an aromatic residue (F) of one monomer (in cyan) with FAD of the opposite monomer (in magenta). The inset shows a close-up of the

superposition of the aromatic-FAD interactions in the displayed structures of GvDTR and CtFNR proteins.

Figure S1

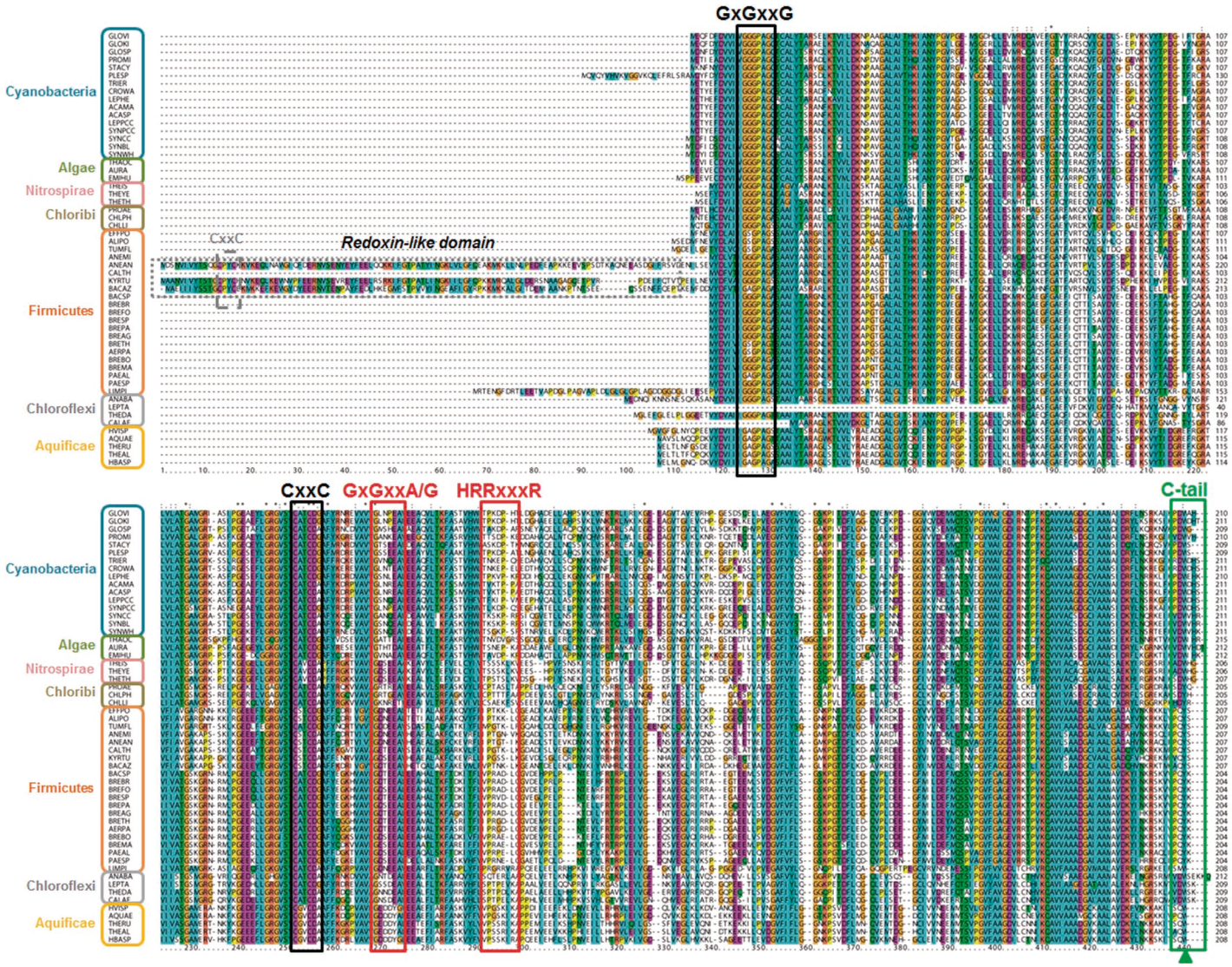
GxGxxG
CxxC
Redoxin-like domain
CxxC
GxGxxA/G
HRRxxxR
C-tail
Cyanobacteria
Algae
Nitrospirae
Chloribi
Firmicutes
Chloroflexi
Aquificae

Figure S2

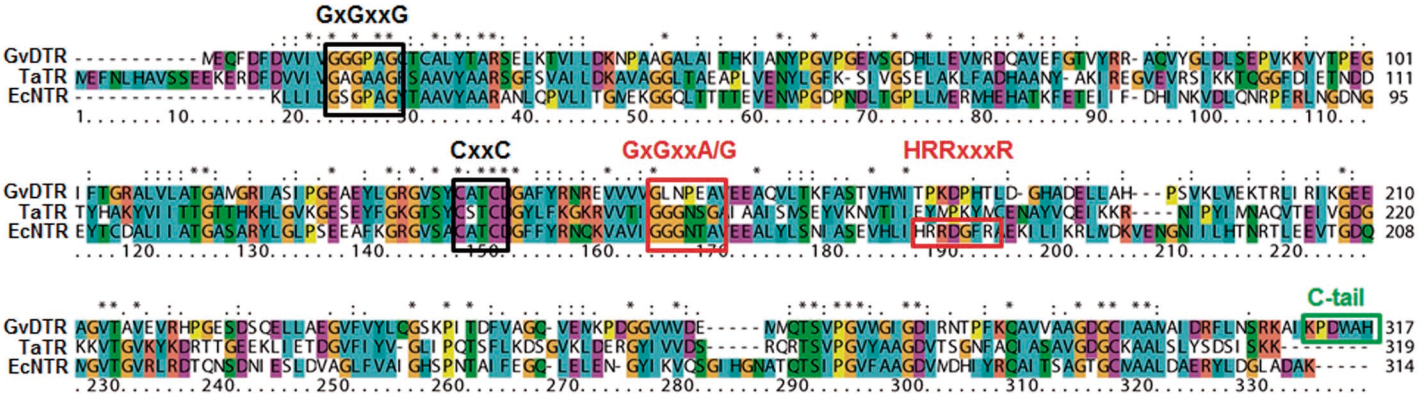

Figure S3

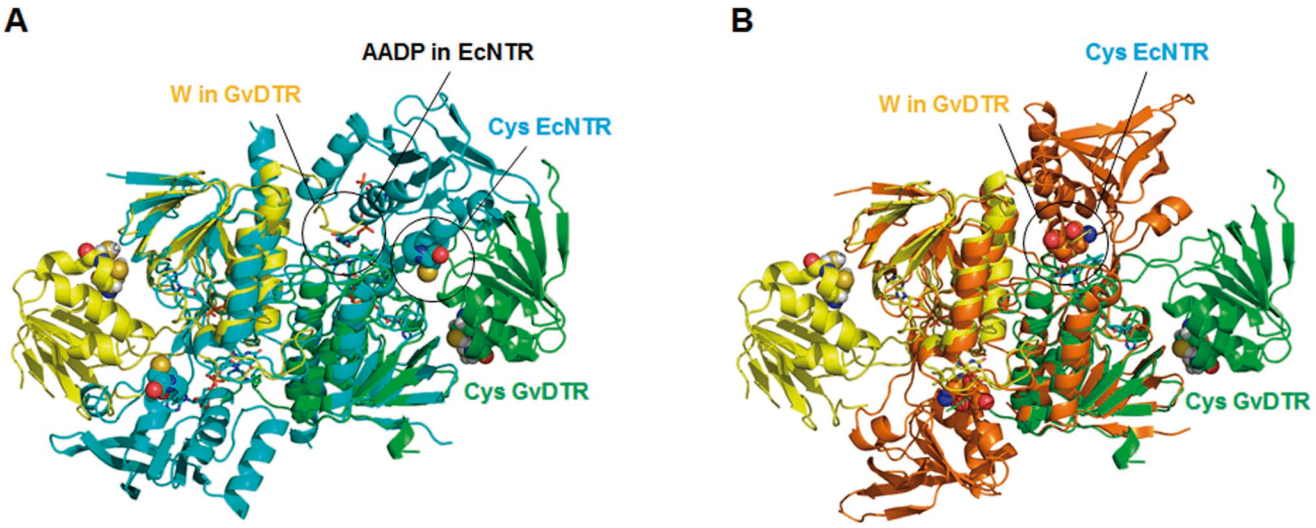
A
AADP in EcNTR
W in GvDTR
Cys EcNTR
Cys GvDTR
B
Cys EcNTR
W in GvDTR
Cys GvDTR

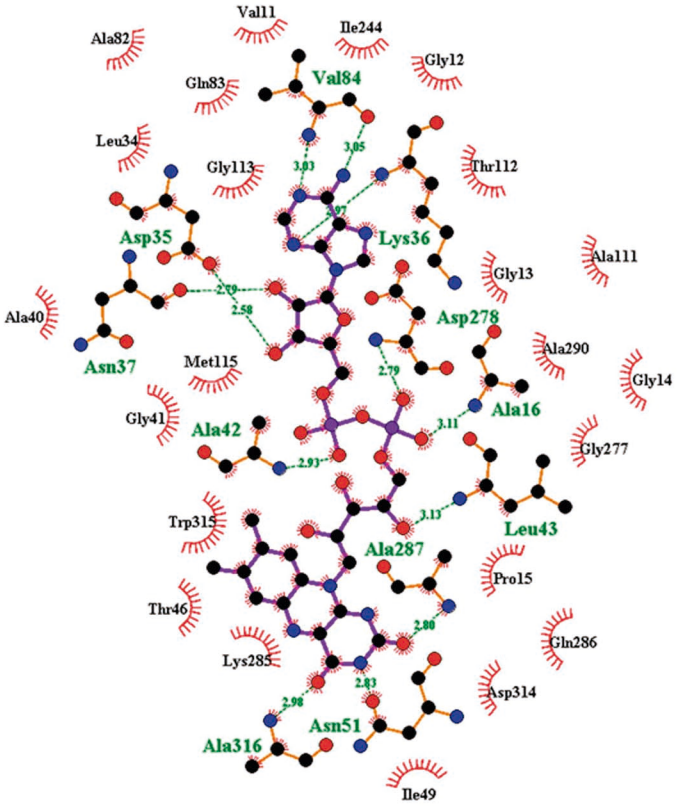
Val11
Ile244
Ala82
Gly12
Gln83
Val84
Leu34
Gly113
Thr112
Asp35
Lys36
Ala111
Gly13
Ala40
Asp278
Ala290
Gly14
Asn37
Met115
Ala16
Gly41
Ala42
Gly277
Trp315
Leu43
Ala287
Pro15
Thr46
Gln286
Lys285
Asp314
Asn51
Ala316
Ile49

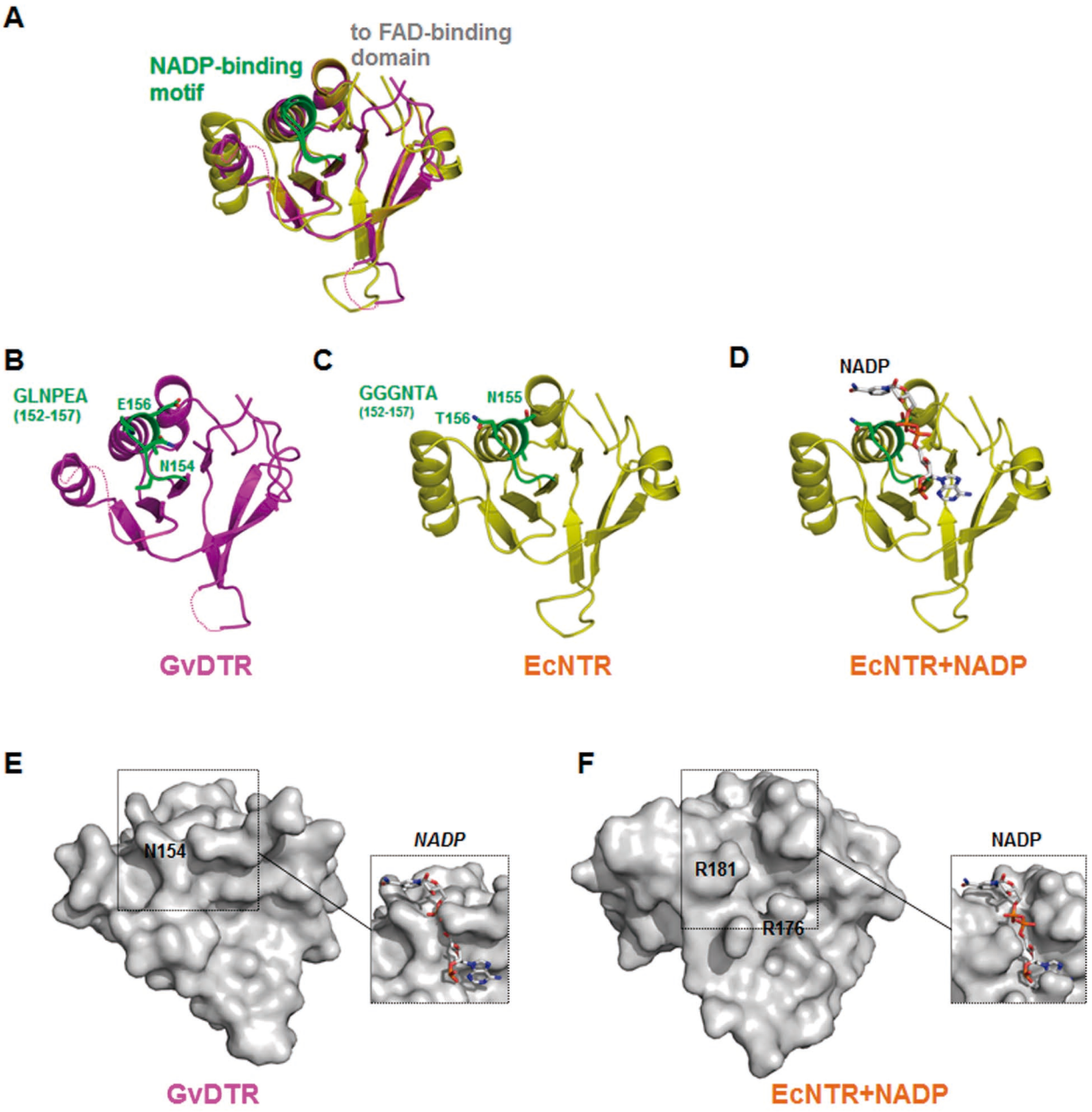
A
NADP-binding motif
to FAD-binding domain
B
GLNPEA (152-157)
E156
N154
GvDTR
C
GGGNTA (152-157)
N155
T156
EcNTR
D
NADP
EcNTR+NADP
E
N154
NADP
GvDTR
F
R181
R176
NADP
EcNTR+NADP

Figure S6